Behavior of cracks in cladded components under consideration of residual stresses

Jörg Hohe[1, a], Marcus Brand[1, b] and Dieter Siegele[1, c]

[1]Fraunhofer Institut für Werkstoffmechanik (IWM)
Wöhlerstr. 11, 79108 Freiburg, Germany

[a]joerg.hohe@iwm.fraunhofer.de, [b]marcus.brand@iwm.fraunhofer.de,
[c]dieter.siegele@iwm.fraunhofer.de

Keywords: Cladding, Fracture behavior, Welding process, Residual stresses, Component tests.

Abstract. The present study is concerned with an experimental and numerical investigation of the behavior of sub-clad and surface cracks in ferritic steels with austenitic (welded) cladding. For this purpose, two component tests have been performed. The residual stress field was determined by means of a high precision numerical simulation of the welding and heat treatment processes. Based on the results, a numerical simulation of the component tests was performed for a fracture mechanics assessment of the situation at crack initiation and arrest. In the present tests, it was observed that failure was initiated in the ferritic range whereas the austenitic cladding remained intact even in the case of a limited crack extension in the base metal.

Introduction

Cladded ferritic pressure vessels with austenitic welded cladding are common in power generation and many other technological fields. In the industrial design process, the fracture assessment of cladded components is usually performed by means of a two-step procedure consisting of a stress analysis of the uncracked component under consideration of the cladding and a subsequent fracture assessment using analytical formulae. In this procedure, the cladding is either assumed to be cracked or neglected (ASME Code [2], German KTA rules [3], etc.). The assumption of a cracked cladding is conservative. Nevertheless, the safety margin cannot easily be quantified. On the other hand, a more detailed numerical analysis under consideration of the cladding might be difficult due to the different failure modes and loads in both materials as well as due to the complex residual stress field caused by the welding and heat treatment processes as well as by the mismatch in the coefficients of thermal expansion.

Aim of the present study is the experimental and numerical investigation of the behavior of cracks in ferritic components supplied with an austenitic welded cladding considering both, sub-clad and through-clad surface cracks. For this purpose, two large-scale specimens consisting of a ferritic pressure vessel steel were cladded with an austenitic material and supplied with a surface and a sub-clad crack respectively. The specimens were tested under combined thermal and mechanical loading conditions (three-point bending). Both specimens failed by a brittle initiation in the ferritic material. For the specimen with through-clad crack, a first initiation with a subsequent crack extension was followed by a crack arrest before final failure occurred at a significantly higher load level. For the specimen with sub-clad crack, no interim crack extension and arrest prior to final failure was observed. In both cases, the cladding remained intact and stable until the ultimate fracture of the specimens.

The local conditions for crack initiation and arrest were analyzed in a numerical simulation of the experiments. In a first analysis, the residual stress field was determined by means of a detailed analysis of the welding process and the subsequent heat treatment process. The residual stress field was found to have a complex periodic character with distinct local variations. In the subsequent analysis of the fracture experiments, it was demonstrated that the brittle failure of the base metal

was the more critical fracture event compared to a possible ductile crack extension into the cladding. The experimental and numerical results were found to be in an excellent agreement.

Material

The base material used in the experimental investigation was a German 22 NiMoCr 3-7 nuclear grade pressure vessel steel similar to A 508 class 2. The material was taken from the cylindrical shell of a reactor pressure vessel originally intended for a power plant that finally has not been constructed. The material was forged followed by a heat treatment consisting of an austenization at T = 900°C. Subsequently, the shell was quenched in water, tempered at T = 650°C for 7.5 h followed by cooling in air. From the available material block, two large plates (700 x 300 x 74 mm) as large scale fracture specimens and three smaller plates (360 x 155 x 55 mm) for fabrication of specimens for the basic characterization of the material were cut. All plates were supplied with a double layer austenitic cladding consisting of CN 24/13 NBR 800 BS for the first layer whereas CrNi 21/10 – BS electrodes were used for the second layer. Both electrodes had a width of 60 mm. The individual layers were 4 mm thick. The cladding process was performed according to the relevant German nuclear standard (KTA 3201 [3]). After the cladding process, the plates were tempered at T = 600°C for 10 h.

Basic Characterization

The basic characterization of the mechanical behavior of the material was performed in tensile tests of round miniature specimens with 2 mm diameter and 20 mm gauge length. The characterization was performed separately for each of the different material zones (base metal, heat affected zone, first and second layer of the cladding) under quasi static conditions throughout the relevant temperature ranges for the component tests and the simulation of the welding process ranging from T = -150°C up to T = 1000°C. The creep response of the material was determined in relaxation tests using slightly larger round tensile specimens. The experiments were performed at temperatures of T = 450°C, 525°C and 600°C. From the relaxation characteristics, the parameters of Norton's creep law were extracted.

For the simulation of the welding process, a further characterization of the material with regard to the thermo physical properties has been performed. In this context, the specific heat capacity, the density, the coefficient of thermal expansion and the thermal conductivity were determined throughout the relevant temperature range for the welding process (ambient temperature to T = 1000°C).

The fracture toughness of the base metal was determined on fracture tests of SE(B) 10 x 10 specimens with a crack depth of a/W = 0.5. For a realistic determination of the fracture toughness of cracks in the ferritic material directly underneath the cladding, two of the small plates were supplied with a 10 mm deep surface crack prior to the cladding process. After the cladding and heat treatment process, the specimens were machined from the pre-cracked plates such that the desired crack depth was achieved. The specimens were tested according to ASTM standard E 1921 [1] in the temperature range between T = -70°C and -90°C. Due to the heat treatment and the position of the specimens in the original plates, a tough behaviour with T_0 = -95.6°C was observed.

Full details on the experimental procedures and the complete set of results can be found in the final report on the respective research project (Hohe et al. [5]).

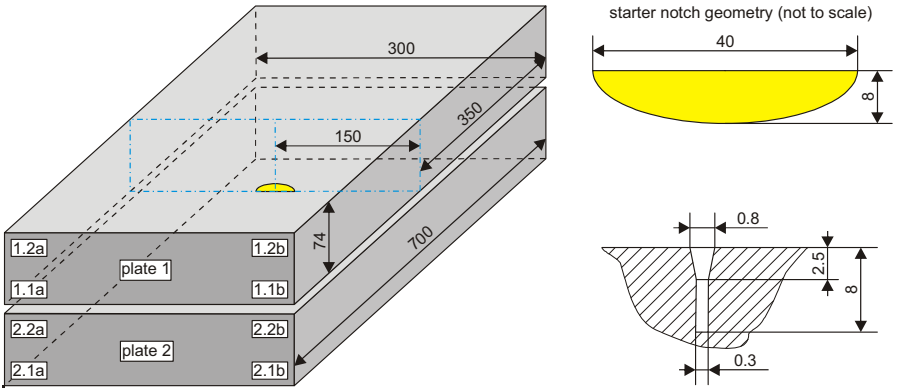

Figure 1: Large-scale fracture mechanics specimens.

Large-scale Fracture Experiments

In the experimental investigation, two large scale plates with semi-elliptical surface cracks according to Fig. 1 were tested. The starter notch for the sub-clad crack was provided prior to cladding by electrical discharge machining. The notch was fatigued under three-point bending with a final load level of approximately $K_I = 20$ MPam$^{1/2}$. Subsequently, the crack was cladded over. The second plate was supplied with a through-clad surface crack by a similar procedure after the cladding and heat treatment. Within the base metal, the starter notch was of similar dimensions as for the specimen with sub-clad crack. After preparation of the cracks, both specimens were machined to a final width of 220 mm.

The specimens were tested under combined thermo-mechanical loading conditions. Similar to a previous experiment (Hodulak et al. [4]), the cracked surface of the specimens was cooled with liquid nitrogen filled into a thermally insulated cooling basin, whereas the opposite surface was kept at higher temperatures by an electrical resistance heating. The heating power was controlled such

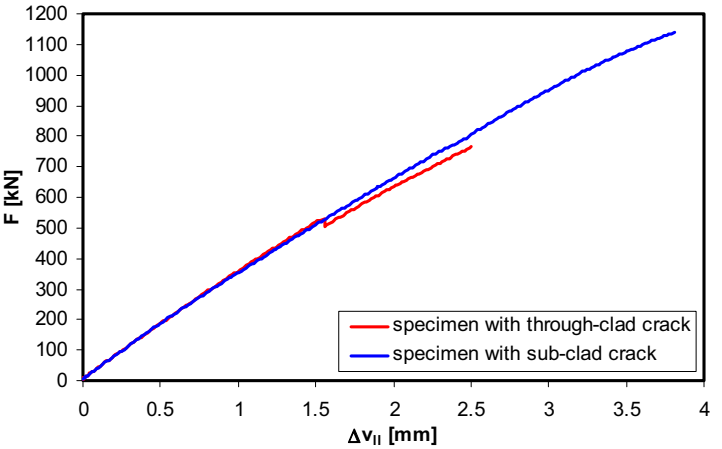

Figure 2: Load-deflection diagram.

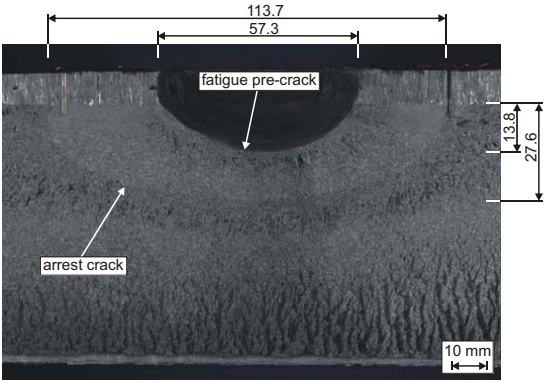

Figure 3: Fracture surface of the specimen with through-clad (surface) crack.

that steady state conditions with a thermal stationary gradient ranging from close to T = -196°C on the cracked surface to ambient temperature at the opposite surface were achieved. Subsequently, the specimens were loaded mechanically to fracture under displacement controlled three point bending.

In Fig 2, the resulting load in both tests is plotted as a function of the bending deformation Δv_{II}. For the specimen with through-clad surface crack, a distinct drop in the resulting load is observed at a displacement of $\Delta v_{II} = 1.553$ mm. The drop in the resulting load was caused by a crack extension in the ferritic material range followed by a crack arrest. During this crack extension, the cladding over the advancing crack remained intact. At $\Delta v_{II} = 2.502$ mm, final fracture of the specimen occurred. The fracture surface of the specimen is presented in Fig. 3. Both, the initial fatigue crack and the arrest crack are clearly visible. The fact that the cladding remained intact during the interim crack extension explains the relatively small drop in the resulting load although the crack surface in the ferritic range increased approximately five times.

For the specimen with sub-clad crack, no distinct interim crack extension was observed prior to final fracture of the specimen at a bending deformation of $\Delta v_{II} = 3.808$ mm and a resulting force of F = 1.139 MN (see Fig. 2 as well as the fracture surface in Fig. 4). The cladding remained stable and intact throughout the mechanical loading phase of the experiment. This visual observation is confirmed by measurements of the relative displacement of two points located on the cracked surface on opposite sides of the crack in comparison to a similar measurement on two points near the side of the specimen outside the influence zone of the crack.

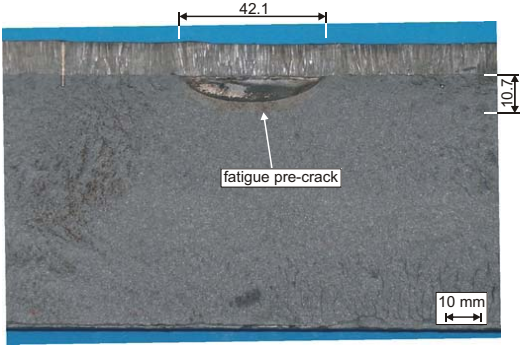

Figure 4: Fracture surface of the specimen with sub-clad crack.

Determination of the Residual Stress Field

For a detailed determination of the residual stress field of the large scale specimens, a numerical simulation of the welding and heat treatment processes has been performed using the finite element method. The simulations were based on a full model of the uncracked plates with a fine resolution of the welding zone. The simulation of the welding process was based on the quasi-static material data whereas the creep data were used in the simulation of the stress relaxation during the post weld heat treatment (see Siegele and Brand [6] for details).

The residual stresses for the rear half of the specimens prior to and after the heat treatment are presented in Fig. 5. The distinct periodic nature of the residual stress field after the welding process is clearly visible in the first row of figures. During the heat treatment, the distinct stress peaks vanish, nevertheless, the residual stress field retains its periodic character. Since the stress relaxation occurs at elevated temperatures, the residual stress level increases again due to the mismatch in the

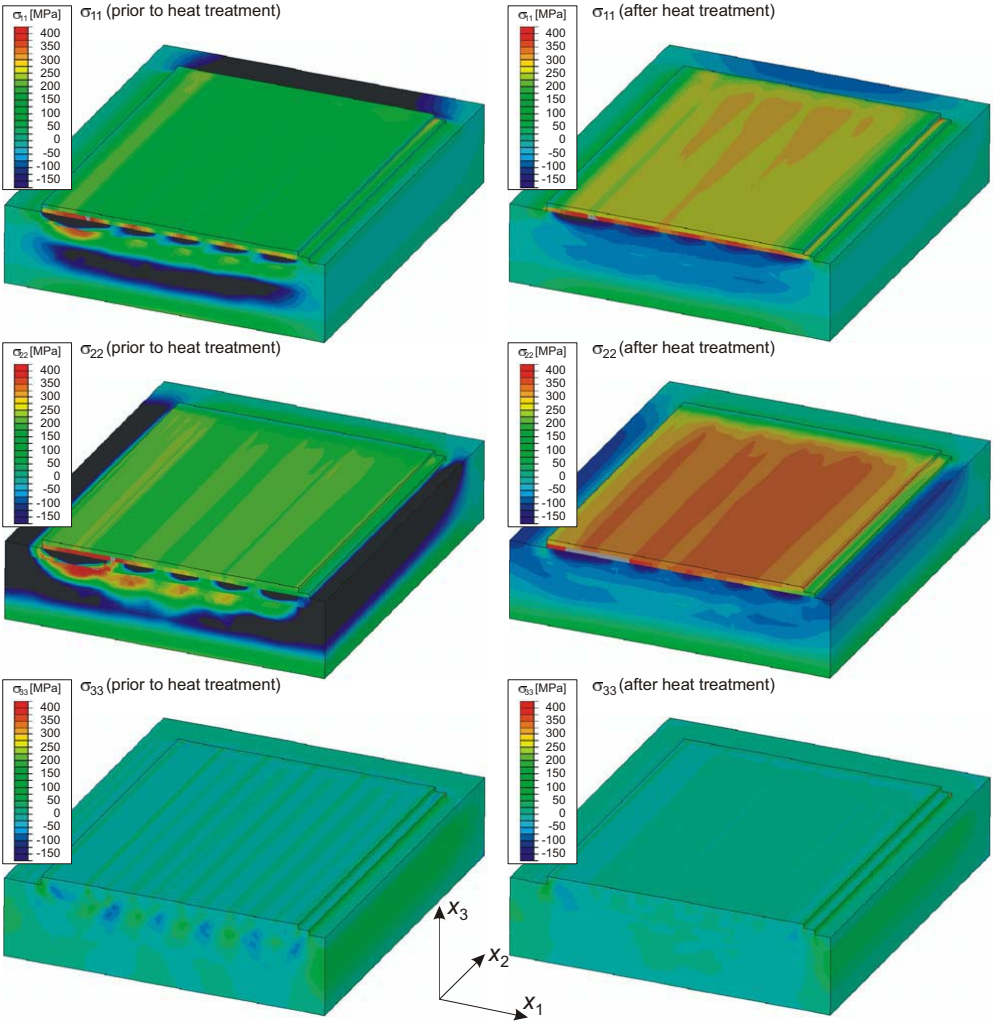

Figure 5: Residual stress field prior to and after post weld heat treatment.

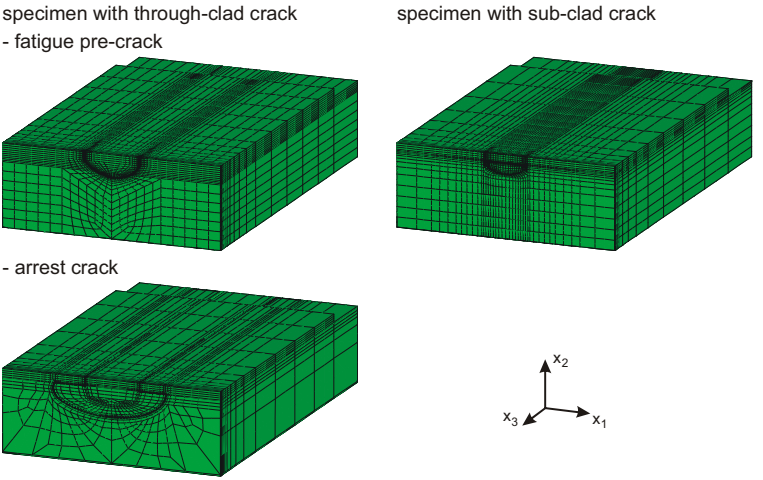

Figure 6: Finite element models for simulation of the fracture experiments.

coefficients of thermal expansion of the base metal and the cladding during cooling down from the heat treatment temperature to ambient temperature. This effect results in an increase of the tensile residual stresses in the cladding during the heat treatment (see Fig. 5).

Simulation of the Fracture Experiments

For the simulation of the fracture experiments, alternative finite element models with a rather fine mesh resolution along the crack fronts considering only the rear half of the specimens have been used. The residual stress fields obtained in the previous simulations were applied as initial conditions for stresses and plastic strain. The employed models are presented in Fig. 6. In this context, two different models have been used for the specimen with through-clad (surface) crack considering the fatigue pre-crack and the arrest crack respectively. Again, the results from the analysis of the first stage of the loading history were transferred as initial conditions onto the model for analysis of the second stage.

In Fig. 7, the computed local stress intensity factors K_J along the crack front within the ferritic material range are presented as a function of the corresponding local temperatures T, considering the instant of the crack extension (fatigue pre-crack and arrest crack) for the specimen with through-clad (surface) crack as well as the instant of final fracture for both specimens. In addition, the fracture toughness curves for 5%. 50% and 95% failure probability according to the master curve concept (ASTM E 1921 [1]) are plotted, using the measured reference temperature of T_0 = -95.6°C.

For the specimen with through-clad (surface) crack, strong variations of the local fracture toughness along the crack front are observed at the instant of the initiation of the original fatigue pre-crack. The highest values are observed in the heat affected zone directly at the ferritic/austenitic interface where the maximum value coincides with the 50% fractile of the master curve concept. At the deepest point of the crack, only rather low failure probabilities are obtained. This result is confirmed by fractographic observations, where the primary initiation spot was detected directly at the ferritic/austenitic interface on the left hand side of the fracture surface presented in Fig. 3. At crack arrest, the level of the local stress intensity factor is far below the initiation toughness curve with a more even distribution along the crack front compared to the situation at initiation. At final fracture, the maximum stress intensity factor K_J again is found in the vicinity of the interface of the

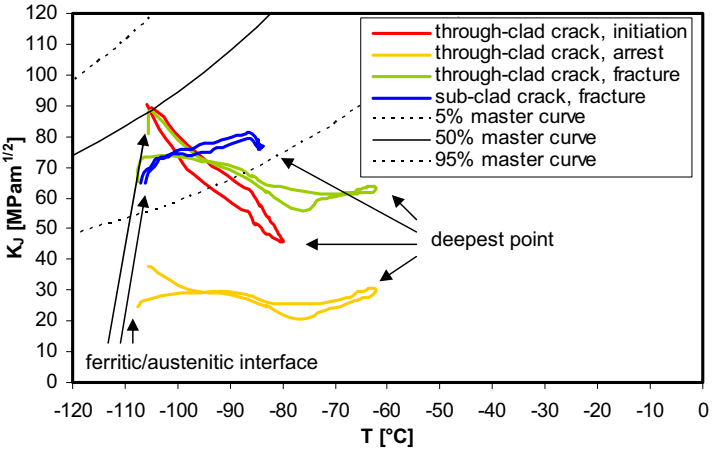

Figure 7: Fracture mechanics assessment of the large scale fracture experiments.

base metal with the cladding. The maximum value is approximately the same as in case of the initiation of the original fatigue pre-crack.

At the instant of final fracture of the specimen with sub-clad crack, a lower local failure probability is obtained, compared to the specimen with through-clad crack. On the other hand, significant failure probabilities are obtained along much larger portions of the crack front, indicating a larger highly loaded material volume. Due to the temperature gradient, the maximum local failure probability ($P_f = 20.6\%$) does not coincide with the position of the maximum stress intensity factor but it is found at a position in the heat affected zone approximately 2 mm below the interface of the ferritic and austenitic material ranges. Again, this result is confirmed by the results of the fractographic investigation, where the cleavage triggering spot was identified with a large sulphide inclusion, located near the crack front, approximately 2 mm below the ferritic/austenitic interface on the right hand side of the fracture surface as presented in Fig. 4.

Conclusions

The objective of the present study was an investigation of the effect of the cladding and the related residual stress field of the fracture behavior of cracks within the base metal of ferritic components supplied with an austenitic cladding. In a combined experimental and numerical approach, it was demonstrated for two crack configurations in large scale specimens that the brittle failure of the ferritic base metal is the more critical fracture event compared to a possible ductile crack extension into the austenitic clad material. In the current experiments, the cladding remained stable throughout the loading history until final failure of the specimens, even in case of a brittle crack extension in the base metal. The numerical results were found in an excellent agreement with the experimental observations.

Acknowledgement

The present work has been financially supported by the German Federal Department of Economics and Technology (BMWi) under grant no. 150 1278.

References

[1] ASTM Standard E 1921-05: *Standard Test Method for Determination of Reference Temperature T_0 for Ferritic Steels in the Transition Range*, American Society for Testing and Materials, West Conshohocken, PA (2005).

[2] *ASME Boiler and Pressure Vessel Code, Sec. XI*, American Society of Mechanical Engineers, New York 1995.

[3] KTA 3201: *Komponenten des Primärkreises von Leichtwasserreaktoren*, Kerntechnischer Ausschuss, Bonn (1997).

[4] L. Hodulak, J.G. Blauel, D. Siegele und B. Urich: Nucl. Eng. Des. Vol. 188 (1999) pp. 139-147.

[5] J. Hohe, M. Brand, D. Siegele, I. Varfolomeev, Y. Sguaizer, J. Schüler, B. Urich, C. Fehrenbach, E. Haas, S. Oeser, M. Möser, V. Varfolomeyeva, S. Luckow und V. Hardenacke: *Bewertung von Rissen in der Plattierung*, Report S35/2007, Fraunhofer Institut für Werkstoffmechanik, Freiburg (2008).

[6] D. Siegele und M. Brand: Proc. 2007 ASME Pressure Vessels and Piping Conf. (San Antonio, TX, 2007), CD-ROM.